Some New Properties of Kelvin-Helmholtz Waves in an Atmosphere With and Without Condensation Effects

F. EINAUDI AND D. P. LALAS[1]

Cooperative Institute for Research in Environmental Sciences,[2] University of Colorado, Boulder 80302

(Manuscript received 1 April 1974, in revised form 2 July 1974)

ABSTRACT

The stability and characteristics of Kelvin-Helmholtz waves in an atmosphere that may be saturated over some of its height are investigated analytically and numerically. It is shown that, if there is a temperature jump at the interface, the Wegener hypothesis, i.e., the assumption that stability boundary curves are loci of neutral waves travelling with phase velocity equal to the mean of the velocities of the regions above and below the discontinuity, is invalid. Instead, the stability boundary corresponds to the singular neutral modes with phase speed equal to the velocity in one or the other layer, depending on the sign of the temperature jump and the presence of saturation. Furthermore, the effect of saturation on the stability is found to be substantial. For the common case of a shallow saturated layer adjacent to the interface, the system is shown to behave essentially as if the temperature jump were smaller by an amount proportional to the mixing ratio and thickness. Finally, the validity of the Boussinesq approximation is examined and is found to be in error by less than 1% for horizontal wavelengths between 10 and 10^4 m.

1. Introduction

Kelvin–Helmholtz waves are those generated at a plane interface between two semi-infinite fluid layers that move with different horizontal velocities, in the presence of gravity. Since the first attempt by Helmholtz to explain billow clouds, models with discontinuities have been extensively used to analyze atmospheric situations in which sharp transitions, from one relatively uniform state of velocity and temperature to another, occur within a layer thin compared to the characteristic wavelengths involved. The Kelvin–Helmholtz waves that are associated with this discontinuous model are thought to be responsible for clear air turbulence in the troposphere and stratosphere (Reiter and Hayman, 1962; Sekioka, 1970), for some kinds of billow clouds and noctilucent clouds (Ludlam, 1967, 1968; Woods, 1968), and for a variety of other phenomena in the oceans and atmospheres.

The original model consisted of two semi-infinite incompressible fluids separated by a horizontal velocity discontinuity, with or without a density discontinuity at the interface. The effect of compressibility was first introduced by Haurwitz (1931, 1932, 1941) in an attempt to obtain a better agreement between observed and computed wavelengths of billow clouds. Compressibility effects, as well as stratification effects, have been included by Grigor'yev and Dokushayev (1971), who, however, analyzed the resulting dispersion relation for special cases only, and by Gossard and Munk (1954).

The objective of this paper is to analyze in detail the eigenvalue equation of the system, to derive the stability boundary separating stable from unstable regions, to describe some new properties of the solutions, and to gauge the effect of condensation. To this end, in Section 2, the governing equations are stated for a dry and saturated atmosphere. In Section 3, some properties of the stability boundaries are proven. In particular, it is shown that the so called Wegener hypothesis (see Sekera, 1948), i.e., the assumption that stability boundary curves are loci of neutral waves travelling with phase velocity equal to the mean of the velocities of the regions above and below the discontinuity, leads to considerable underestimation of the largest unstable wavelength. In Section 4, the results of numerical calculations of neutral boundaries, growth rates and phase velocities of waves are presented and discussed, for dry and saturated atmospheres. Finally, in Section 5, we attempt to make the model more physically realistic by inserting in the classical two-semi-infinite-layer model a third shallow saturated layer adjacent to the interface, and discuss the resulting changes to the eigenvalue problem.

2. The hydrodynamic equations and the resulting eigenvalue problem

The motion of a perturbation to a horizontally homogeneous but height-dependent atmosphere with

[1] On leave from the Department of Mechanical Engineering Sciences, Wayne State University, Detroit, Mich.

[2] University of Colorado/National Oceanic and Atmospheric Administration.

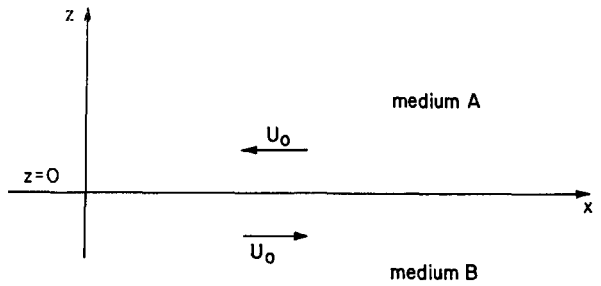

FIG. 1. The geometry of the system. The top semi-infinite layer is always dry, whereas the bottom layer may be saturated throughout.

background temperature $T_0(z)$, density $\rho_0(z)$, pressure $p_0(z)$ and velocity $\mathbf{q}=q(z)\hat{\mathbf{e}}_x$ is governed by the following equations:

$$\frac{d}{dt}\rho+\rho_0\left(\frac{\partial}{\partial x}u+\frac{\partial}{\partial z}w\right)+w\frac{d}{dz}\rho_0=0 \tag{1}$$

$$\rho_0\frac{d}{dt}u+\frac{\partial}{\partial x}p+\rho_0 w\frac{d}{dz}q=0 \tag{2}$$

$$\rho_0\frac{d}{dt}w+\frac{\partial}{\partial z}p+\rho g=0 \tag{3}$$

$$\rho_0 c_v^{(1)}\frac{d}{dt}T+p_0\left(\frac{\partial}{\partial x}u+\frac{\partial}{\partial z}w\right)=0 \tag{4}$$

$$p=R^{(1)}(T_0\rho+\rho_0 T). \tag{5}$$

In the above, p, ρ, u, w and T are the perturbation pressure, density, horizontal velocity, vertical velocity and temperature, respectively, while $c_v^{(1)}$ is the specific heat at constant volume, $R^{(1)}$ the gas constant for dry air, and g the gravitational acceleration acting in the negative z direction. The operator d/dt is given by

$$\frac{d}{dt}=\frac{\partial}{\partial t}+q\frac{\partial}{\partial x}. \tag{6}$$

For the configuration to be considered first, shown in Fig. 1, the system of equations (1)–(5) holds for both upper and lower semi-infinite regions. If suffix A refers to the top and B to the bottom half-space, the background velocities are given by

$$\left.\begin{aligned}\mathbf{q}_A&=-U_0\hat{\mathbf{e}}_x\\ \mathbf{q}_B&=U_0\hat{\mathbf{e}}_x\end{aligned}\right\}, \tag{7}$$

where U_0 is a constant and $\hat{\mathbf{e}}_x$ is the unit vector in the x direction. The background temperatures T_{0A} and T_{0B} are constant in each half-space but may or may not be continuous across the interface at $z=0$.

We study the stability of this system by assuming that the perturbations are of the form

$$\left.\begin{aligned}p(x,z,t)&=P\exp[i\theta-z/(2H)]\\ \rho(x,z,t)&=R\exp[i\theta-z/(2H)]\\ u(x,z,t)&=U\exp[i\theta+z/(2H)]\\ w(x,z,t)&=W\exp[i\theta+z/(2H)]\\ \theta&=\omega t-k_x x-kz\\ \omega&=\omega_r+i\omega_i\end{aligned}\right\}, \tag{8}$$

where ω is the frequency of oscillation; $\lambda_x=2\pi/k_x$ and $\lambda_z=2\pi/k$, the horizontal and vertical wavelengths, respectively; $H=R^{(1)}T_0/g$ is the scale height for an isothermal atmosphere; and P, R, U, W are each constant.

Eliminating the temperature from (4) through the use of (5), and using Eq. (8), one obtains a linear, homogeneous system of four equations in the four unknowns P, R, U and W. By setting the determinant of the coefficients equal to zero, we obtain the dispersion relation for either layer

$$\Omega^4-\Omega^2c^2(k_x^2+k^2)+c^2n^2k_x^2-\Omega^2c^2/(4H^2)=0, \tag{9}$$

where the Doppler frequency Ω, the sound speed c, and the Brunt–Väisälä frequency n are given by

$$\Omega=\omega-k_x q, \tag{10}$$

$$c^2=R^{(1)}T_0\left(1+\frac{R^{(1)}}{c_v^{(1)}}\right), \tag{11a}$$

$$n^2=-g\left(\frac{g}{c^2}+\frac{1}{\rho_0}\frac{d\rho_0}{dz}\right). \tag{12}$$

Since many observations of Kelvin–Helmholtz waves are accompanied by billow clouds, it is of interest to include the influence of saturated water vapor and resultant phase changes. As it will be shown later, this effect on the dynamic stability of the system is substantial and has to be taken into account in analyses of wave characteristics from billow cloud observations. This can be accomplished by simply replacing the expression for the sound speed (11a) with

$$c^2=R^{(1)}T_0\left[1+\frac{R^{(1)}/c_v^{(1)}}{1+\left(\frac{L_v}{R^{(2)}T_0}\right)^2\frac{R^{(2)}}{c_v^{(1)}}\delta}\right], \tag{11b}$$

where $R^{(2)}$ is the gas constant for water vapor, L_v the latent heat of evaporation, and δ is the mixing ratio, i.e., the ratio of water vapor to dry air densities. Eq. (11b) reduces to (11a) when no phase change occurs. Eq. (12) remains unchanged, but with c^2 given now by (11b). Detailed derivation of (11b) and a discussion of the approximations involved can be found in Lalas and Einaudi (1973, 1974). It is valid for an atmosphere with enough liquid water content to remain saturated throughout the whole cycle of the wave fluctuations.

It should also be mentioned that in deriving Eq. (9), c^2 has been treated as a constant, implying, therefore, that δ is constant with height. Since T_0 is constant in each half-space, by the Clausius–Clapeyron equation, ρ_{0v}, the water vapor background density, is also a constant, while by the hydrostatic equation and the relation $p_0=R^{(1)}T_0\rho_0$, $\rho_0\sim\exp(-z/H)$. Since by definition $\delta=\rho_{0v}/\rho_0$, it follows that $\delta\sim\exp(z/H)$. If δ is to be considered a constant, the attenuation rate in the z direction or the vertical wavelength or both, have to be small compared with the scale height H. This point has been checked in the numerical calculations carried out.

Using Eq. (7) and introducing the normalized frequency φ,

$$\varphi=\omega/(k_xU_0)=\varphi_r+i\varphi_i, \tag{13}$$

we rewrite Eq. (9) in an equivalent form, for each half-space:

$$k_A=\pm\frac{k_xU_0}{c_A}\left\{(\varphi+1)^2-\frac{c_A^2}{U_0^2}\left[1+\frac{1}{4H_A^2k_x^2}-\frac{n_A^2}{k_x^2U_0^2}\frac{1}{(\varphi+1)^2}\right]\right\}^{\frac{1}{2}} \tag{14}$$

$$k_B=\pm\frac{k_xU_0}{c_B}\left\{(\varphi-1)^2-\frac{c_B^2}{U_0^2}\left[1+\frac{1}{4H_B^2k_x^2}-\frac{n_B^2}{k_x^2U_0^2}\frac{1}{(\varphi-1)^2}\right]\right\}^{\frac{1}{2}}. \tag{15}$$

The radiation conditions at $z=\pm\infty$ determine the sign in (14) and (15); we must have

$$\mathrm{Im}(k_A)<0, \quad \mathrm{Im}(k_B)>0. \tag{16}$$

If k_A or k_B or both are real, the sign is chosen so as to insure that the direction of energy propagation, as indicated by the group velocity, is away from the interface.

Finally, the boundary conditions at the displaced interface between the two half-spaces demand (i) that the vertical displacements ξ_A and ξ_B calculated on both sides of the interface be equal, which results, to first order, in the condition

$$\frac{W_A}{\omega+k_xU_0}=\frac{W_B}{\omega-k_xU_0}, \tag{17}$$

and (ii) that the total pressure matches across the displaced interface, which, again to first approximation, requires

$$ig\rho_{0A}\frac{W_A}{(\omega+k_xU_0)}+P_A=ig\rho_{0B}\frac{W_B}{(\omega-k_xU_0)}+P_B, \tag{18}$$

where ρ_{0A} and ρ_{0B} are calculated at $z=0$.

From the two above equations, one obtains the dispersion relation for the entire system:

$$r\left\{g-k_x^2U_0^2\frac{(\varphi+1)^2-[n_A^2/(k_x^2U_0^2)]}{\frac{g}{c_A^2}-\frac{1}{2H_A}-ik_A}\right\}=g-k_x^2U_0^2\frac{(\varphi-1)^2-[n_B^2/(k_x^2U_0^2)]}{\frac{g}{c_B^2}-\frac{1}{2H_B}-ik_B}, \tag{19}$$

where

$$r=(\rho_{0A}/\rho_{0B})_{z=0}=T_{0B}/T_{0A}. \tag{20}$$

Eq. (19), when k_A and k_B are eliminated via the use of (14) and (15), is an equation between k_x and φ, if the background quantities for each medium are given. It could be used to find the allowable values of φ for a given wavenumber k_x and thus the phase velocity and attenuation or growth of a perturbation of the form (8). In its present form, it includes the effects of both compressibility and stratification, as well as of the possible influence of condensation.

3. Analysis of the eigenvalue equation: Analytical considerations

For the wavelengths and velocities of interest in our case, that is λ_x of the order of meters or larger and velocities of the order of meters per second, the Boussinesq approximation generally holds and considerably simplifies Eqs. (14), (15) and (19) to

$$k_A=\pm\frac{k_x}{(\varphi+1)}\left[\frac{n_A^2}{U_0^2k_x^2}-(\varphi+1)^2\right]^{\frac{1}{2}}, \tag{21}$$

$$k_B=\pm\frac{k_x}{(\varphi-1)}\left[\frac{n_B^2}{U_0^2k_x^2}-(\varphi-1)^2\right]^{\frac{1}{2}}, \tag{22}$$

$$r\left\{g+\frac{k_x^2U_0^2}{ik_A}\left[(\varphi+1)^2-\frac{n_A^2}{U_0^2k_x^2}\right]\right\}=\left\{g+\frac{k_x^2U_0^2}{ik_B}\left[(\varphi-1)^2-\frac{n_B^2}{U_0^2k_x^2}\right]\right\}. \tag{23}$$

Later numerical analysis showed that indeed our results were insensitive to the inclusion of the neglected compressibility terms.

Before discussing the results of the numerical analysis of (23), we will prove some important properties that became apparent in the course of this investigation: If the stability boundary is defined as a curve in the (U_0,λ_x) plane separating unstable ($\omega_i<0$) solutions from stable ones ($\omega_i=0$), then:

(i) For $\Delta T=T_{0A}-T_{0B}=0$ and no condensation, the stability boundary in the (U_0,λ_x) plane corresponds

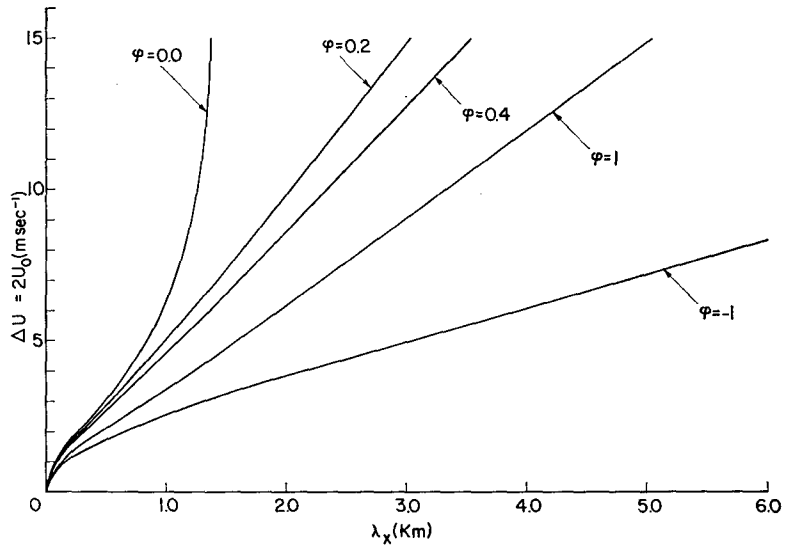

FIG. 2. Some of the neutral curves ($\omega_i=0$) for $T_{0A}=281$K, $T_{0B}=280$K, and mixing ratio $\delta=0.03$.

to $\varphi=0$, and therefore the principle of exchange of stabilities holds in the sense that $\omega_r/\omega_i\to 0$ as $\omega_i\to 0_+$ (see Drazin and Howard, 1961; Chandrasekhar, 1961; Miles, 1963).

(ii) For $\Delta T=0$ and with the B layer saturated throughout, the stability boundary corresponds to $0<|\varphi|<1$. In particular, $\varphi=0$ or $|\varphi|=1$ can never correspond to a stability boundary.

(iii) For $\Delta T\neq 0$, the stability boundary always corresponds to either $\varphi=1$ or $\varphi=-1$.

Let us mention here that since on the stability boundary $\omega_i=0$, stability boundary curves are also called neutral curves. It should be recalled, however, that neutral curves ($\omega_i=0$) exist which are not stability boundaries. In addition, it should be noted that for $\Delta T\neq 0$ the stability boundaries correspond to singular neutral modes; this is not the case when $\Delta T=0$.

Let us first prove points (i) and (ii). Since $\Delta T=0$, $\rho_{0A}=\rho_{0B}$ and Eq. (23) can now be written as

$$\frac{1}{k_A}\left[(\varphi+1)^2-\frac{n_A^2}{k_x^2U_0^2}\right]=\frac{1}{k_B}\left[(\varphi-1)^2-\frac{n_B^2}{k_x^2U_0^2}\right]. \quad (24)$$

Squaring, we obtain

$$8\varphi^3-\varphi^2(n_A^2-n_B^2)/(k_x^2U_0^2)+\varphi[8-2(n_A^2+n_B^2)/(k_x^2U_0^2)]-(n_A^2-n_B^2)/(k_x^2U_0^2)=0. \quad (25)$$

By squaring, of course, one introduces extra roots which in general do not satisfy the original equation.

If neither medium is saturated, $n_A=n_B=n$, and Eq. (25) reduces to

$$\varphi\left[\varphi^2+1-\frac{n^2}{2k_x^2U_0^2}\right]=0, \quad (26)$$

which has the two solutions

$$\varphi=0, \quad (27)$$

$$\varphi=\pm[n^2/(2k_x^2U_0^2)-1]^{\frac{1}{2}}. \quad (28)$$

The solution $\varphi=0$, given by (27), does not infer any functional relation between k_x and U_0; Eq. (28), on the other hand, reveals that the transition from φ imaginary to φ real takes place when

$$n^2/(2k_x^2U_0^2)=1, \quad \text{i.e.,} \quad \varphi=0, \quad (29)$$

so that Eq. (29) is indeed the neutral curve and $\varphi=0$ is the corresponding value of φ.

When saturation occurs, for $\Delta T=0$, $n_A\neq n_B$ and $\varphi=0$ is not a solution of (25) or (24). The solutions of (25) are given by the standard third-order algebraic equation expressions:

$$\varphi=(s_1+s_2)+\frac{(n_A^2-n_B^2)}{(24k_x^2U_0^2)},$$

$$\varphi=-\tfrac{1}{2}(s_1+s_2)+\left(\frac{n_A^2-n_B^2}{24k_x^2U_0^2}\right)\pm i\frac{\sqrt{3}}{2}(s_1-s_2),$$

where

$$s_1=[a+(b^3+a^2)^{\frac{1}{2}}]^{\frac{1}{3}}, \quad s_2=[a-(b^3+a^2)^{\frac{1}{2}}]^{\frac{1}{3}},$$

with

$$b=\tfrac{1}{3}[1-(n_A^2+n_B^2)/(4k_x^2U_0^2)]-\frac{1}{9}\left[\frac{n_A^2-n_B^2}{8k_x^2U_0^2}\right]^2,$$

$$a=-\tfrac{1}{6}[1-(n_A^2+n_B^2)/(4k_x^2U_0^2)]\times[(n_A^2-n_B^2)/(8k_x^2U_0^2)]+(n_A^2-n_B^2)/(16k_x^2U_0^2)+(1/27)[(n_A^2-n_B^2)/8k_x^2U_0^2]^3.$$

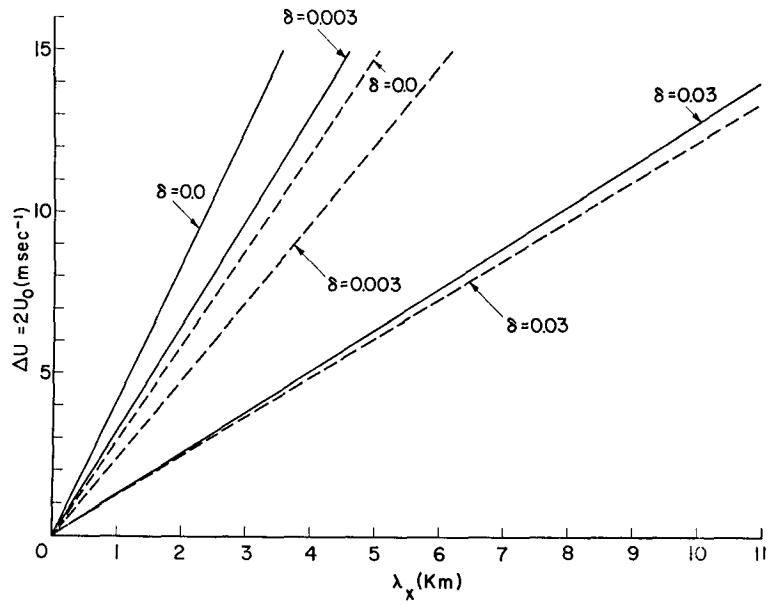

FIG. 3. Stability boundary curves for $T_{0B}=280$K, $\Delta T=T_{0A}-T_{0B}=0$ (solid lines) and $\Delta T=0.1$K, dashed lines. Three values for δ (0.0, 0.003, 0.03) are indicated.

Now one can see that all three solutions are real only if s_1 and s_2 are complex conjugates, which holds when $b^3+a^2<0$. The neutral boundary then is given by the condition $b^3+a^2=0$, with

$$\varphi=\varphi_r=-a^{\frac{1}{3}}+(n_A^2-n_B^2)/(24k_x^2U_0^2).$$

The values of φ_r, given by the above expression, can be shown to lie between -1 and 1 and be different from zero.

In order to prove (iii), we introduce the notation

$$k_A=k_{Ar}+ik_{Ai}, \quad k_B=k_{Br}+ik_{Bi}. \tag{30}$$

We now take the real and imaginary part of (23); in the two resulting equations we set $\omega_i=0$, obtaining

$$g(r-1)-rU_0^2k_{Ai}(\varphi_r+1)^2=-U_0^2k_{Bi}(\varphi_r-1)^2, \tag{31}$$

$$rk_{Ar}(\varphi_r+1)^2=k_{Br}(\varphi_r-1)^2. \tag{32}$$

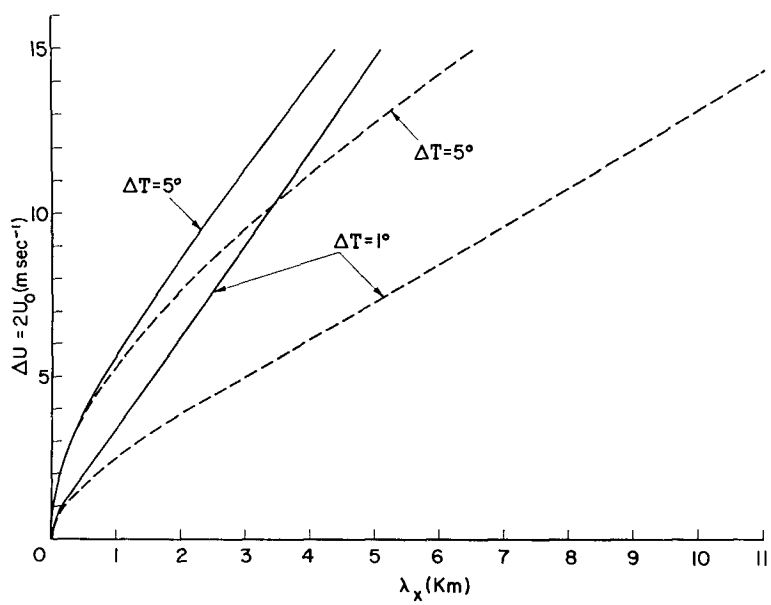

FIG. 4. As in Fig. 3 except for $\Delta T=1$K and $\Delta T=5$K. The two values for δ (0.0, 0.03) are considered.

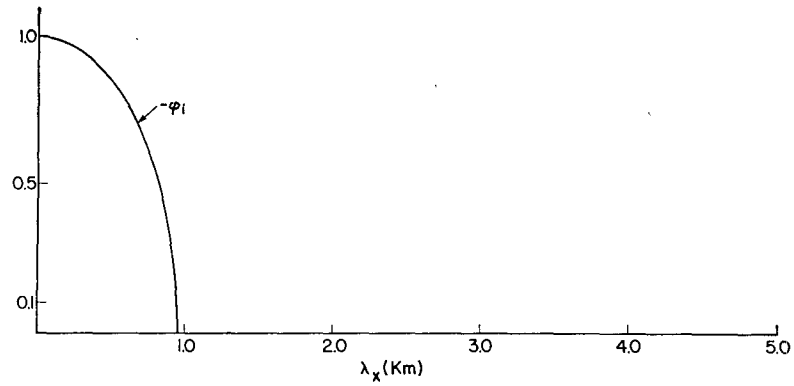

FIG. 5. Normalized growth rates $-\varphi_i=-\omega_i/(k_xU_0)$ and normalized phase velocity $\varphi_r=\omega_r/(k_xU_0)$ vs horizontal wavelength λ_x; $T_{0A}=T_{cB}$ and $\delta=0$.

One should notice that for real φ, k_A and k_B are either real or purely imaginary. Eqs. (31) and (32) define, in general, a family of neutral curves characterized by $\varphi=\varphi_r$, real, and the stability boundary belongs to this family.

Since k_A is either real or purely imaginary, let us first take

$$n_A^2/(k_x^2U_0^2)<(\varphi+1)^2, \tag{33}$$

which implies

$$k_{Ar}=0. \tag{34}$$

To satisfy (32) then, either

$$\varphi_r=1 \tag{35a}$$

or

$$k_{Br}=0. \tag{35b}$$

Taking the first alternative and substituting $\varphi_r=1$ into (31), we obtain, with the use of (21) with the appropriate sign,

$$g(r-1)+4rU_0^2k_x[1-n_A^2/(4k_x^2U_0^2)]^{\frac{1}{2}}=0, \tag{36}$$

which defines k_x in terms of U_0. If we now choose the alternative (35b), then Eq. (31), using (16), (21) and (22), can be written as

$$g(r-1)+rU_0^2k_x(\varphi_r+1)[(\varphi_r+1)^2-n_A^2/(k_x^2U_0^2)]^{\frac{1}{2}} =-U_0^2k_x|\varphi_r-1|[(\varphi_r-1)^2-n_B^2/(k_x^2U_0^2)]^{\frac{1}{2}}. \tag{37}$$

Eq. (37) defines a family of neutral curves in the (U_0,λ_x) plane with φ_r as a parameter; it reduces to (36) if we set $\varphi_r=1$. The whole family of curves for values of φ_r between -1 and 1 is bounded from the right by the $\varphi_r=-1$ curve, as is shown in Fig. 2.

Similarly, when $[n_A^2/(k_x^2U_0^2)]>(\varphi+1)^2$ so that

$$k_{Ai}=0, \tag{38}$$

(31) reduces to

$$g(r-1)=-U_0^2k_{Bi}(\varphi_r-1)^2. \tag{39}$$

Since $r\neq1$, the right-hand side must be non-zero so $k_{Bi}\neq0$ and

$$k_{Br}=0. \tag{40}$$

The right-hand side of (32) is now zero so that $\varphi_r=-1$, and (39) reduces to

$$g(r-1)+4U_0^2k_x[1-n_B^2/(4k_x^2U_0^2)]^{\frac{1}{2}}=0. \tag{41}$$

All the neutral curves for values of φ_r between -1 and 1

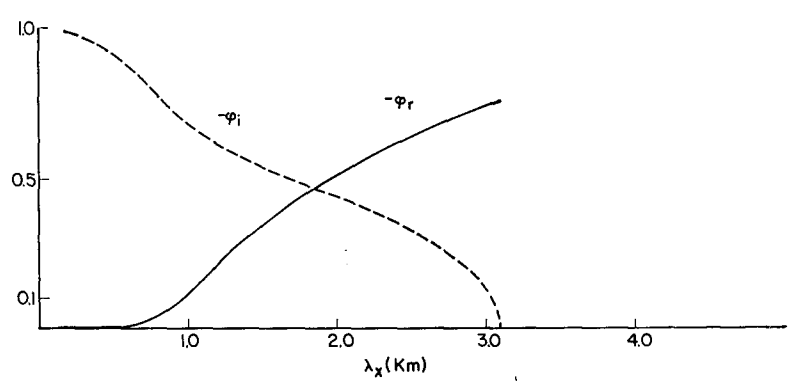

FIG. 6. As in Fig. 5 except for $\delta=0.03$.

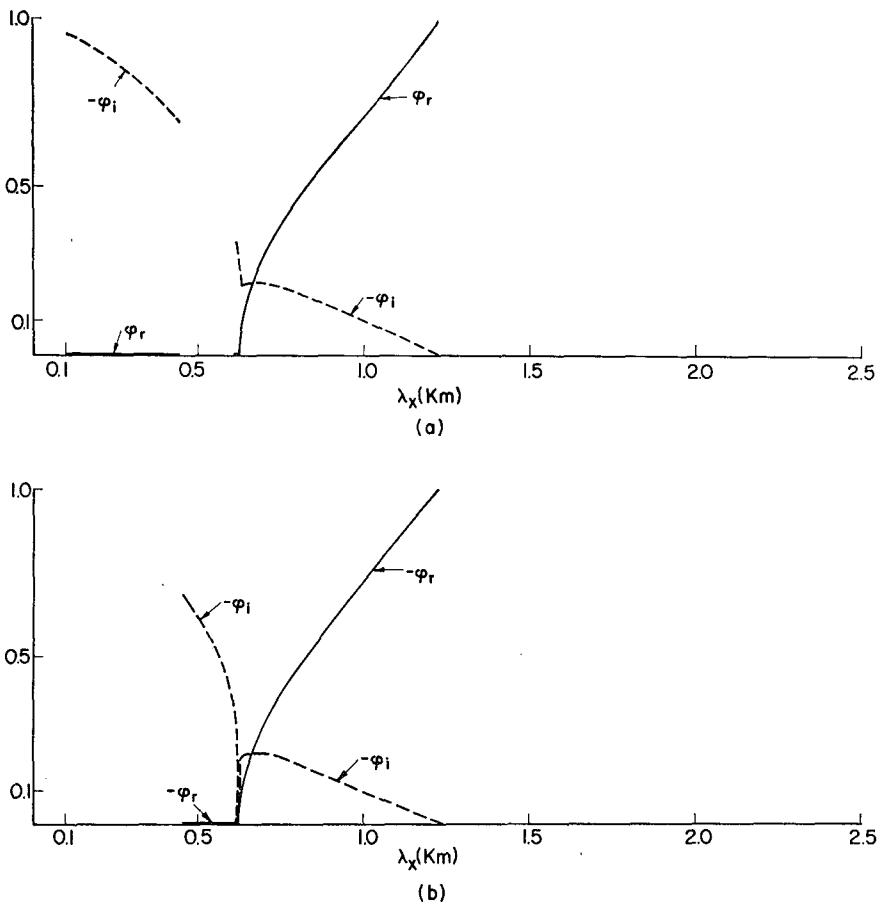

FIG. 7. Values of φ for $T_{0B}=280$K, $T_{0A}=281$K, $\delta=0$ and $U_0=2$ m sec^{-1} as a function of λ_x: (a) $\varphi_r>0$, (b) $\varphi_r<0$.

are then given by either (36) or (37) or (41). No other neutral curve exists.

To establish the stability boundary, only the range $0\leqslant|\varphi_r|\leqslant 1$ has to be considered, because of the semicircle theorem. We have established that the neutral curves for $\varphi=1$ and $\varphi=-1$, obtained from Eqs. (36) and (41), correspond to the largest neutral wavelength, for given velocity. It remains to be shown that complex eigenvalues exist adjacent to such curves $\varphi=\pm 1$. A perturbation analysis about $\varphi=1$ indicates that a small decrease of φ_r to a value less than 1 demands the existence of a small imaginary part for φ, while a small increase of φ_r past 1 requires $\varphi_i=0$. Similarly, a small increase of φ_r past -1, demands the existence of a small imaginary part for φ, while a small decrease to values less than -1, requires $\varphi_i=0$. Thus complex eigenvalues exist to the left, but not to the right of the $\varphi=\pm 1$ curves.

The stability boundary then will be either $\varphi=1$ or $\varphi=-1$, depending on which one gives the rightmost curve in the (U_0,λ_x) plane. For the case illustrated in Fig. 2, the $\varphi=-1$ curve is the appropriate one.

4. Some numerical results

The identification of the unstable wavelengths and the calculation of the corresponding growth rates and phase velocities are the two main objectives of the numerical analysis. The numerical calculations are carried out for a velocity difference between the two layers equal to $\Delta U_0=2U_0$ as shown in Fig. 1, and for a constant temperature $T_{0B}=280$K in the bottom layer. The temperature in the top layer is equal to $T_{0A}=T_{0B}+\Delta T$, with ΔT always positive. Furthermore, when saturation occurs, it is always the bottom layer that is saturated throughout.

The stability boundaries are plotted in Figs. 3 and 4. They have been calculated, with the considerations of the previous section in mind, but without the use of the Boussinesq approximation, i.e., with all the compressibility terms included.

Comparing the stability boundary curves with the same humidity, but with different ΔT, one sees that an increase of ΔT, making the upper layer lighter, does not necessarily increase the stability of the system for all wavelengths. Instead, it increases the stability

for small wavelengths, but decreases it for large wavelengths.

Condensation, on the other hand, always destabilizes the system and increases the largest unstable wavelength, by a factor of 2 in some cases when $\delta=0.03$, which is a large value for the mixing ratio. The relative effect of condensation is reduced when ΔT is larger, but is always present.

Normalized growth rates $\varphi_i=\omega_i/(k_xU_0)$ and phase velocities $\varphi_r=\omega_r/(k_xU_0)$ for the unstable wavelengths are plotted in Figs. 5–12.

Let us first focus on the $\Delta T=0$ cases shown in Figs. 5 and 6. When, additionally, $\delta=0$, φ_r is zero, and this is indeed the case when the Wegener hypothesis holds and leads to the correct range of unstable wavelengths, as shown in Fig. 5. But the presence of saturated water vapor throughout the bottom layer B significantly alters growth rates and phase velocities and renders the Wegener hypothesis invalid. As indicated in Fig. 6, for $\delta=0.03$, the stability boundary corresponds to $\varphi_r\approx0.76$ rather than $\varphi_r=0$ as in the dry case, and the unstable range is tripled.

Turning now to the case $\Delta T\neq0$, one notices that, regardless of condensation, two modes are usually present, one with φ_r positive, the other with φ_r negative. But ranges of wavelengths λ_x exist where only one mode with $\varphi_i\neq0$ is present and others over which no mode with $\varphi_i\neq0$ is present. For $\Delta T\neq0$ or $\delta\neq0$ or both, the Wegener hypothesis leads to largest unstable wavelengths of 0.614, 0.769, 1.667, 1.247, 0.266 and 0.275 km, for the configurations shown in Figs. 7, 8, 9, 10, 11 and 12, respectively. All these wavelengths do not belong to the stability boundaries. The effect of water vapor on both φ_i and φ_r is substantial, especially for small values of ΔT.

Figs. 5, 6, 9, 10, 11 and 12 were obtained using the Boussinesq approximation. Comparison of the largest unstable wavelengths with values from Fig. 4, reveals that the use of the Boussinesq approximation introduces an error less than 1%. The effect of the Boussinesq approximation on the growth rates is of the same order, while the qualitative behavior remains the same; this can be seen from Figs. 7 and 8 that were computed without the Boussinesq approximation. In view of the above considerations, the most unstable wavelengths computed in the manner described in this paper will be larger than those computed using the Wegener hypothesis and neglecting condensation effects. Haurwitz

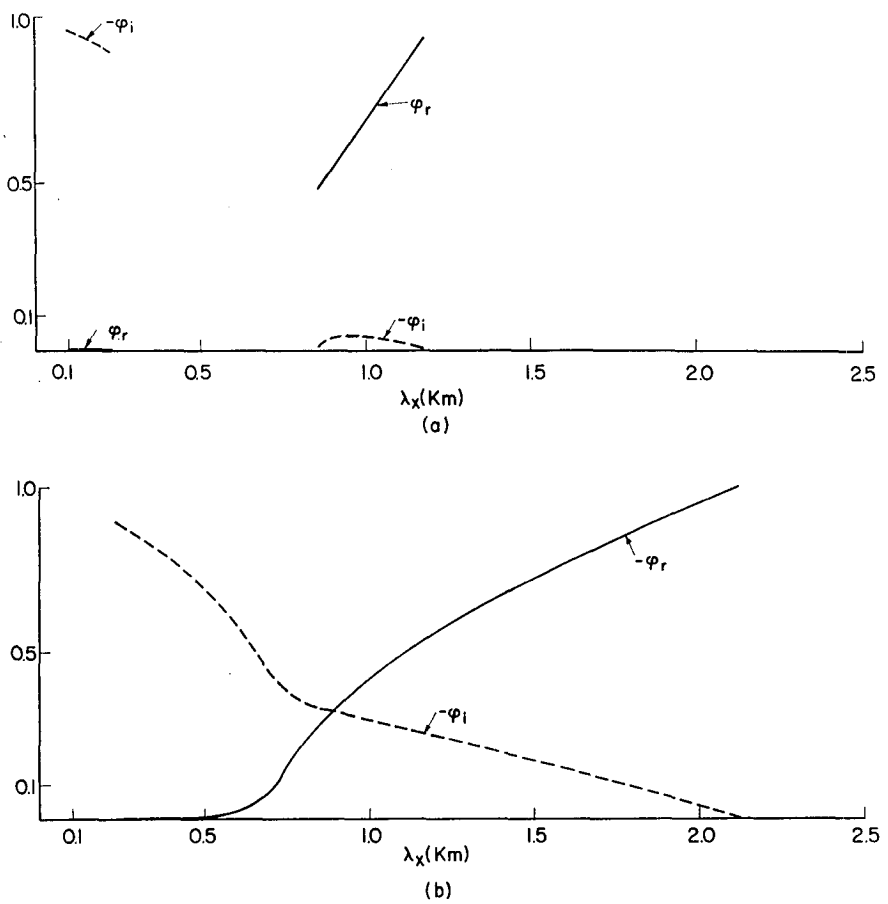

FIG. 8. As in Fig. 7 except for $\delta=0.03$.

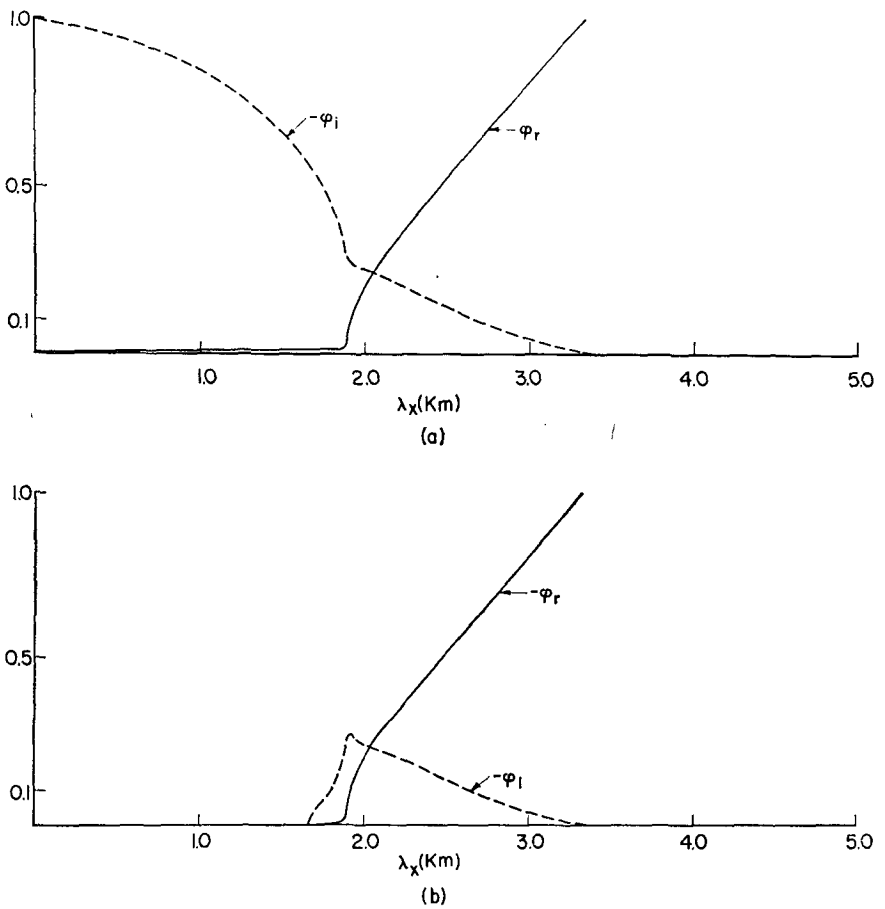

FIG. 9. Values of φ for $T_{0B}=280$K, $T_{0A}=281$K, $\delta=0$ and $U_0=5$ m sec^{-1} as a function of λ_x: (a) $\varphi_r>0$, (b) $\varphi_r<0$.

(1941), using the latter method, calculated wavelengths for nine observations of billow clouds. His computed values are in much better agreement with the observed ones than the values one would obtain assuming an incompressible atmosphere. Yet, in six cases out of nine, his values are, to various degrees, still smaller than the observed ones. The points brought out in this paper would improve the agreement in these cases.

5. The effect of finite depth of the saturated region

Kelvin–Helmholtz waves are often accompanied by saturation in the form of billow clouds (Ludlam, 1968) that are usually of shallow depth, and are often used to infer wave properties. In many other instances of shear wave instabilities (Gossard, 1962; Hooke and Hardy, 1974), clouds are present. In these situations, saturation in the atmosphere occurs over a relatively narrow height range away from the ground, since at lower heights the temperature is too high for the available water vapor to reach saturation and at larger heights the water vapor content is too low (a notable exception, of course, is fog). In an effort to model the true atmosphere more closely, we will next consider the situation shown in Fig. 13, i.e., three layers, the top denoted by A and the bottom denoted by B, both semi-infinite, unsaturated, and the middle denoted by $\tilde{\text{B}}$ of thickness L, taken to be saturated. The background velocities and temperatures of layers B and $\tilde{\text{B}}$ are the same so that $T_{0B}=T_{0\tilde{B}}$, and the only difference is that $n_B{}^2\neq n_{\tilde{B}}{}^2$, because of the saturation effects in layer $\tilde{\text{B}}$. Similar three-layer models, with linear shear in the middle layer but with no humidity, have been studied by Gossard (1974). The still more realistic case of the middle layer being near saturation and being brought to saturation by the wave itself, is currently under investigation by the authors.

Eqs. (1)–(5) still apply in all three layers, and so does the form of the perturbation quantities given by Eqs. (8). The only difference is the fact that both an upgoing and a downgoing wave now exist in layer $\tilde{\text{B}}$. Thus, boundary conditions have to be satisfied at both $z=0$ and $z=-L$ as well as the radiation conditions at infinity. Furthermore, we will utilize the Boussinesq approximation from the start.

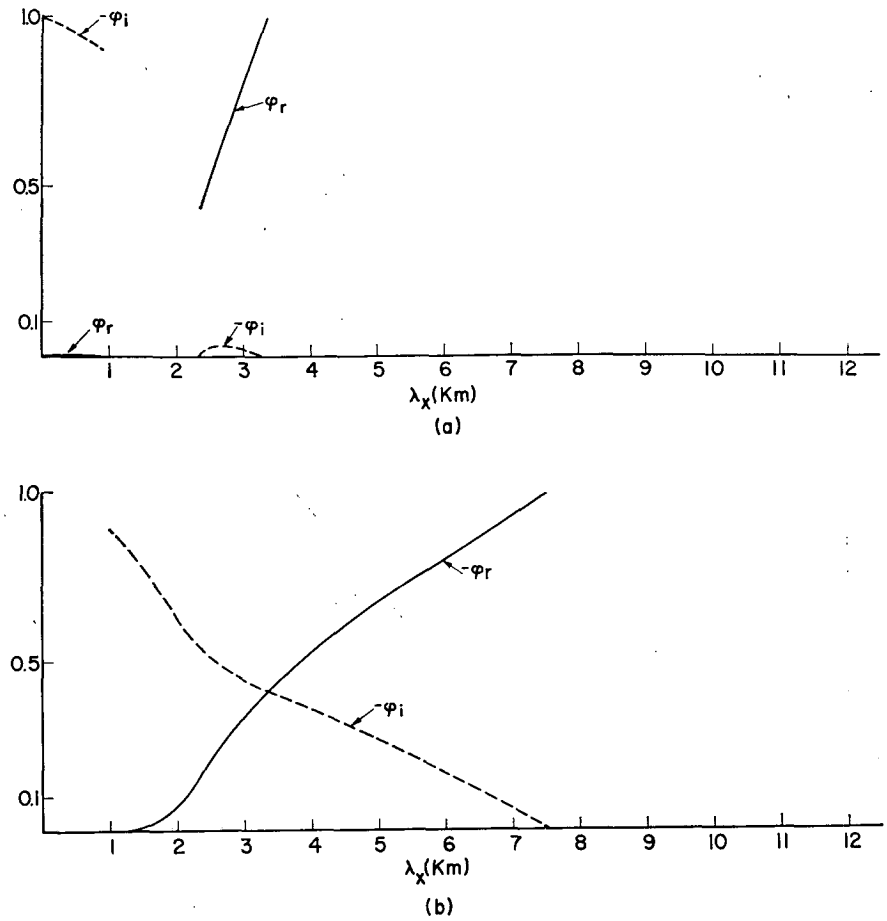

FIG. 10. As in Fig. 9 except for $\delta=0.03$.

The resulting eigenvalue problem is then given by

$$r\left[g+k_x^2U_0^2\frac{(\varphi+1)^2-[n_A^2/(k_x^2U_0^2)]}{ik_A}\right]$$

$$=g+k_x^2U_0^2\left[\frac{(\varphi-1)^2-n_{\tilde{B}}^2/(k_x^2U_0^2)}{ik_{\tilde{B}}}\right]\left(\frac{\Xi-1}{\Xi+1}\right), \quad (42)$$

$$\frac{(\varphi-1)^2-[n_B^2/(k_x^2U_0^2)]}{ik_B}$$

$$=\frac{(\varphi-1)^2-[n_{\tilde{B}}^2/(k_x^2U_0^2)]}{ik_{\tilde{B}}}\left[\frac{\Xi\exp(2ik_{\tilde{B}}L)-1}{\Xi\exp(2ik_{\tilde{B}}L)+1}\right], \quad (43)$$

along with (21), (22) and

$$k_{\tilde{B}}=\pm\frac{k_x}{(\varphi-1)}\left[\frac{n_{\tilde{B}}^2}{U_0^2k_x^2}-(\varphi-1)^2\right]^{\frac{1}{2}}, \quad (44)$$

defining k_A, $k_{\tilde{B}}$ and k_B. The sign of k_A is picked so that the wave satisfies the radiation condition at $+\infty$, k_B so that it satisfies the radiation condition at $-\infty$, and the sign of $k_{\tilde{B}}$, by choice, so that it would satisfy the radiation condition at $-\infty$ if the $\tilde{B}$ layer were semi-infinite. Eq. (42) results from imposing the boundary conditions at $z=0$ and (43) from the boundary conditions at $z=-L$. Ξ is the ratio of the amplitudes of the downgoing to the upgoing waves in the $\tilde{B}$ layer. In Eq. (42), $r=\rho_{0A}/\rho_{0\tilde{B}}=T_{0B}/T_{0A}$. The system (42)–(44) along with (21) and (22) reduces to the previous case when L goes to either infinity, or zero.

We will discuss here only the case

$$|k_{\tilde{B}}|L\ll 1, \quad (45)$$

which is appropriate for billow clouds (Ludlam, 1967). In this limit, (43) reduces to

$$\frac{(\varphi-1)^2-[n_B^2/(k_x^2U_0^2)]}{ik_B}$$

$$=\frac{(\varphi-1)^2-[n_{\tilde{B}}^2/(k_x^2U_0^2)]}{ik_{\tilde{B}}}\left[\frac{\Xi(1+2ik_{\tilde{B}}L)-1}{\Xi(1+2ik_{\tilde{B}}L)+1}\right], \quad (46)$$

and elimination of Ξ between (46) and (42) gives

$$g(r-1)-L(n_{\tilde{B}}^2-n_B^2)+rk_x^2U_0^2\frac{[(\varphi+1)^2-n_A^2/(k_x^2U_0^2)]}{ik_A}=k_x^2U_0^2\frac{[(\varphi-1)^2-n_B^2/(k_x^2U_0^2)]}{ik_B}. \quad (47)$$

Rewriting (23) here for convenience

$$g(r-1)+rk_x^2U_0^2\frac{[(\varphi+1)^2-n_A^2/(k_x^2U_0^2)]}{ik_A}=k_x^2U_0^2\frac{[(\varphi-1)^2-n_B^2/(k_x^2U_0^2)]}{ik_B}, \quad (23)$$

and comparing it with (47), we see that the only difference is the extra term $-L(n_{\tilde{B}}^2-n_B^2)$ in the left-hand side. The term $g(r-1)$ is due to the temperature jump across the interface and is negative, for the statically stable configuration of $T_{0A}>T_{0B}$. Since condensation decreases the Brunt-Väisälä frequency, $n_{\tilde{B}}^2<n_B^2$ so that $g(r-1)-L(n_{\tilde{B}}^2-n_B^2)>g(r-1)$. Thus, the effect of a small layer at saturation next to the shear interface is equivalent to reducing the temperature jump across the interface. The essence of our previous considerations remains valid, but with an effective temperature jump equal to

$$\Delta\tilde{T}=\Delta T-\frac{LT_{0A}}{g}(n_B^2-n_{\tilde{B}}^2). \quad (48)$$

For $\delta=0.03$ and $T_{0B}=280$K, the temperature difference is decreased by 1K for every 123 m of saturated layer thickness, while for $\delta=0.001$, a very modest value of the mixing ratio, the temperature difference is decreased by 1K for every 308 m. Using $\Delta\tilde{T}$ given by (48), we can calculate the growth rates and phase velocities as in the case of two semi-infinite layers, as long as (45) is verified.

For the cases when (45) is no longer valid, we resorted to further numerical calculations based on (42) and (43). The growth rates and stability boundaries were

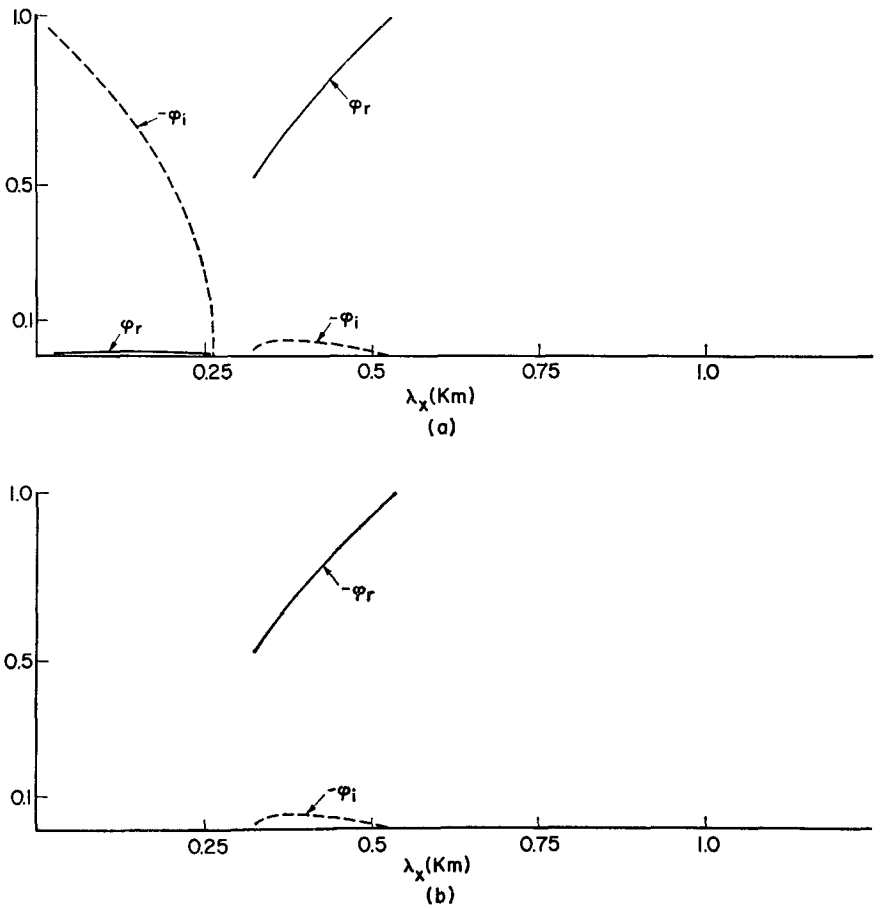

FIG. 11. Values of φ for $T_{0B}=280$K, $T_{0A}=285$K, $\delta=0$ and $U_0=2$ m sec^{-1} as a function of λ_x: (a) $\varphi_r>0$, (b) $\varphi_r<0$.

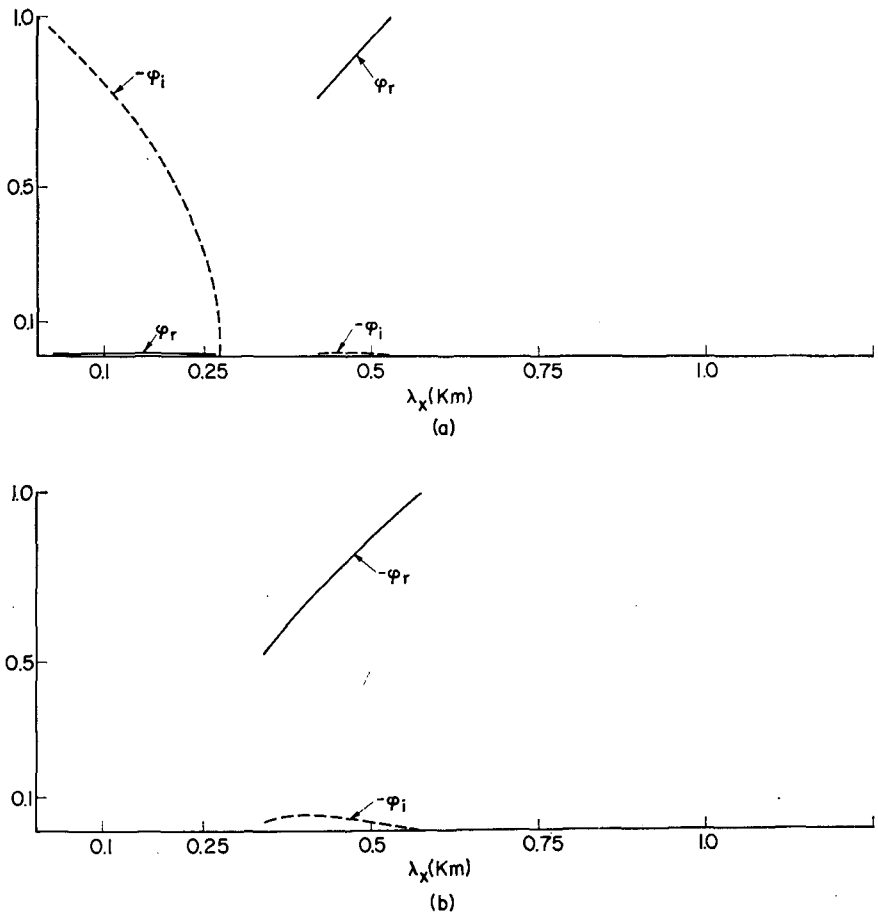

FIG. 12. As in Fig. 11 except for $\delta=0.03$.

then found to lie between the corresponding dry-dry and dry-saturated semi-infinite-layers results. The increase in growth rates depends largely on the thickness of the saturated layer. For example, for the case depicted in Figs. (7a,b) and (8a, b), the largest unstable wavelength was 1230 m for two semi-infinite dry layers and 2120 m for two semi-infinite dry-wet layers. For a finite layer of 500 m thickness with $\delta=0.01$, the largest unstable wavelength was 1980 m, bounded by 1230 and 2120 m.

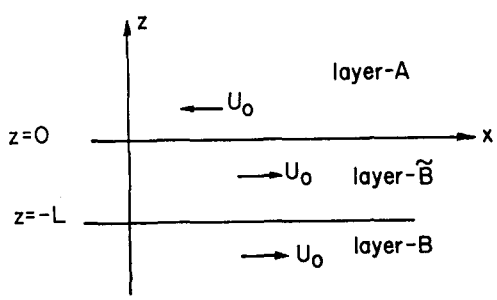

FIG. 13. The geometry of the three-layer system. The middle layer is the only one saturated.

6. Conclusions

The results of this investigation of the stability criteria and growth rates of Kelvin–Helmholtz waves in an atmosphere that may contain saturated regions, can be summarized as follows:

1) The Wegener hypothesis is valid only if there is no temperature jump at the interface and no saturation present. If a temperature jump occurs, regardless of the presence or absence of saturation, the stability boundary is obtained by putting the phase velocity equal to $\pm U_0$, depending on the sign of ΔT and the presence of saturation.

2) The use of the Boussinesq approximation for velocity jumps $\gtrsim 15$ m sec^{-1} and wavelengths between 10 and 10^4 m gives results for the stability boundary and growth rates that are within 1% of the solution of the full compressible equations.

3) The effect of saturation on the stability of the system is substantial, especially for small temperature jumps. When saturation is limited to a shallow layer adjacent to the interface, the system behaves as if the temperature jump were decreased, with growth rates

and stability boundaries lying between the dry-dry and dry-saturated infinite-layer results.

Acknowledgments. This research was supported in part by Grants GA-32604 and GA-40243, both of which are from the National Science Foundation.

REFERENCES

Chandrasekhar, S., 1961: *Hydrodynamic and Hydromagnetic Stability*. Oxford, Clarendon Press, Chaps. 1 and 9.

Drazin, P. G., and L. N. Howard, 1961: Stability in a continuously stratified fluid. *Proc. ASCE, Eng. Mech. Div.*, **87**, 101–116.

Gossard, E. E., 1962: Vertical flux of energy into the lower ionosphere from internal gravity waves generated in the troposphere. *J. Geophys. Res.*, **67**, 745–757.

——, 1974: Dynamic stability of an isentropic shear layer in a statically stable medium. *J. Atmos. Sci.*, **31**, 483–492.

——, and W. Munk, 1954: On gravity waves in the atmosphere. *J. Meteor.*, **11**, 259–269.

Grigor'yev, G. I., and V. P. Dokuchayev, 1971: The instability of a tangential discontinuity in an isothermal atmosphere. *Izv. Atmos. Oceanic Phys.*, **7**, 1093–1095.

Haurwitz, B., 1931: Über die Wellenlänge von Luftwogen. *Beitr. Geophys.*, **34**, 213–232.

——, 1932: Über die Wellenlänge von Luftwogen (2. Mitteilung). *Beitr. Geophys.*, **37**, 16–24.

——, 1941: *Dynamic Meteorology*. New York, McGraw-Hill, Chap. 14.

Hooke, W. H., and K. Hardy, 1974: Further studies of the atmospheric gravity waves over the eastern seaboard on March 18, 1969. Submitted for publication in *J. Appl. Meteor.*

Lalas, D. P., and F. Einaudi, 1973: On the stability of a moist atmosphere in the presence of a background wind. *J. Atmos. Sci.*, **30**, 795–800.

——, and ——, 1974: On the correct use of the wet adiabatic lapse rate in stability criteria of a saturated atmosphere. *J. Appl. Meteor.*, **13**, 318–324.

Ludlam, F. H., 1967: Characteristics of billow clouds and their relation to clear-air turbulence. *Quart. J. Roy. Meteor. Soc.*, **93**, 419–435.

——, 1968: Reply. *Quart. J. Roy. Meteor. Soc.*, **94**, 210.

Miles, J. W., 1963: On the stability of heterogeneous shear flows. Part 2. *J. Fluid Mech.*, **16**, 209–227.

Reiter, E. R., and R. W. Hayman, 1962: On the nature of clear air turbulence (CAT). Atmos. Sci. Paper No. 28, Colorado State University, 41 pp.

Sekera, Z., 1948: Helmholtz waves in a linear temperature field with vertical wind shear. *J. Meteor.*, **5**, 93–102.

Sekioka, M., 1970: Application of Kelvin-Helmholtz instability to clear air turbulence. *J. Appl. Meteor.*, **9**, 896–899.

Woods, J. D., 1968: On the formation of certain billow clouds. *Quart. J. Roy. Meteor. Soc.*, **94**, 209–210.